Photochemical Aging of Secondary Organic Aerosol Particles Generated from the Oxidation of d-Limonene

Maggie L. Walser, Jiho Park, Anthony L. Gomez, Ashley R. Russell, and Sergey A. Nizkorodov*

Department of Chemistry, University of California, Irvine, Irvine, California 92617-2025

Received: September 25, 2006; In Final Form: January 13, 2007

Secondary organic aerosol (SOA) particles are generated by reacting d-limonene vapor and ozone in a Teflon reaction chamber. The reaction is carried out in either dry or humid air in darkness. The resulting SOA particles are collected on glass fiber filters, and their photochemical properties are probed using a combination of UV photodissociation action spectroscopy and absorption spectroscopy techniques. Photolysis of limonene SOA in the tropospheric actinic region (λ > 295 nm) readily produces formic acid and formaldehyde as gas-phase products. The UV wavelength dependence of the photolysis product yield suggests that the primary absorbers in SOA particles are organic peroxides. The relative humidity maintained during SOA particle growth is found to have little effect on the UV wavelength dependence of the photolysis product yield. The data suggest that direct photodissociation processes may play an important role in photochemical processing of atmospheric SOA particles.

Introduction

Atmospheric aerosol particles play an important role in controlling global climate and air quality.[1−6] Studies have shown that as much as 90% of urban aerosol can be organic in nature, making organic aerosol particles and their chemistry of particular interest to atmospheric scientists.[7−16] A large fraction of organic aerosol particles are formed as secondary organic aerosol (SOA) resulting from the condensation of partially oxidized volatile organic compounds (VOC).

In the United States, on a regional scale, biogenic emissions of VOCs tend to be about 3 times higher than anthropogenic emissions. Monoterpenes, which are unsaturated hydrocarbons emitted by certain plants, are responsible for a significant fraction of biogenic VOC emissions.[17] Atmospheric oxidation of carbon−carbon double bonds in monoterpenes produces a variety of polyfunctional species, including alcohols, aldehydes, ketones, and carboxylic acids, which generally have lower vapor pressures than the parent terpenes and can condense to form aerosol particles. As early as 1960, the involvement of terpenes in the formation of tropospheric particles was recognized by Went, who observed a blue haze formed by pine needles in the presence of O_3 in a bell jar.[18] Since that time, SOA yields, reaction mechanisms, and particle composition have been extensively studied for ozonolysis of monoterpenes in smog chambers[19−33] and in simulated indoor environments.[34−39]

To date, the majority of studies of terpene oxidation by O_3, OH, and NO_3 have focused on identifying gas- and condensed-phase products[40,41] and on determining how various factors, such as relative humidity, UV radiation, and NO_x concentration, affect the aerosol yield.[31−33,42] Significant progress has been made in identifying chemical species present in the particle phase, but it has yet to be determined how a particle's composition evolves in the atmosphere as a result of photochemical processes occurring inside and on the surface of the particle.

Once SOA particles are formed, they undergo both physical and chemical aging processes, which may result in large effects on the physicochemical properties of the particles, including their toxicity and ability to nucleate raindroplets. Atmospheric particles are exposed to sunlight 8−14 h a day, therefore, photochemical processes are likely to be among the primary aging mechanisms. The direct effects of solar UV-radiation on the composition and chemistry of monoterpene-derived SOA are currently unknown. However, recent laboratory observations of a reduction of SOA yields in the presence of UV radiation give strong evidence for the potential importance of such processes.[31,33,43−45]

This work focuses on three aspects of the photochemical aging of model SOA particles resulting from the oxidation of d-limonene vapor by ozone. The first is an experimental investigation of the absorption of radiation in the actinic region of the solar spectrum (λ > 295 nm) by SOA particles. The second is an identification of possible photochemical processes occurring within the particles. The third is an estimation of the extent to which such photochemical processes can efficiently compete with other organic aerosol aging and removal processes in the atmosphere.

Experimental

Model SOA particles were formed from the ozone-initiated oxidation of d-limonene vapor in an inflatable Teflon reaction chamber (Figure 1). A fan was used to ensure rapid mixing of ozone and limonene in the chamber. The chamber was first filled to approximately 250 L with dry purified air or, for experiments performed at increased relative humidity (RH), with air from a Nafion humidifier. Ozone, produced by flowing oxygen (99.994% purity) through a commercial ozone generator, was added to the reaction chamber to achieve a concentration of ∼300 ppm. Once the desired relative humidity and ozone concentration were achieved, a 50 sccm (standard cubic centimeters per minute) air flow saturated with d-limonene (97% purity, Fisher Scien-

* To whom correspondence should be addressed. E-mail: nizkorod@uci.edu.

10.1021/jp066293l CCC: $37.00
Published on Web 02/21/2007

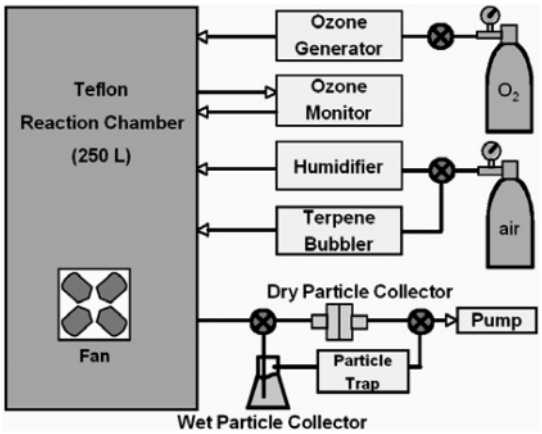

Figure 1. Aerosol generation setup. Limonene is allowed to react with ozone for 1 h in the dark before particle collection. The particles are extracted in polar or nonpolar solvents for UV/vis analysis or are collected on glass fiber filters for IR−CRDS analysis.

tific) was injected into the chamber over the course of 20 min. Saturated vapor was obtained by flowing air through a temperature-controlled bubbler containing limonene at $T = 298$ K (partial pressure of d-limonene = 260 Pa). In the absence of ozone, the final concentration of limonene in the 250-L chamber would be ∼8 ppm, but this level was not achieved because oxidation and particle growth occurred in parallel with limonene addition. The resulting mixture was allowed to age in the dark, at room temperature (∼298 K) and ambient pressure (∼750 Torr), for ∼1 h before particle collection.

The UV/vis absorption spectra of SOA particles were obtained in one of the following ways. The "wet particle collector" (Figure 1) was used to capture and dissolve particles in a nonpolar solvent by bubbling the aerosol/gas mixture from the reaction chamber through a flask filled with CH_2Cl_2. The particle size distribution was measured before and after the collector using a scanning mobility particle sizer (SMPS) to quantify the fraction of the collected particles. The size distribution did not change dramatically, indicating that the wet collector did not preferentially capture specific particle sizes. As a specific example, the mean particle diameter was 315 nm and the total particle number concentration was 4.1×10^5 cm^{-3} before the collector. After the collector, the mean diameter was 321 nm, and the total particle concentration was reduced to 3.4×10^5 cm^{-3} suggesting that ∼17% of the particles were captured by the solvent.

In the second approach ("dry particle collector"), the particles were first collected on a glass fiber filter over the course of ∼10 min and then were ultrasonically extracted with either polar (methanol) or nonpolar (CH_2Cl_2) solvent. The particle filter collection efficiency was measured to be >95% for particles larger than 0.1 μm. Exposure to ambient light was minimized during the collection and extraction processes. As opposed to the wet collector, the extracts prepared this way were less likely to entrap gas-phase components of the reaction mixture. Absorption spectra were recorded in standard 1-cm quartz cuvettes using a Varian Cary 50 UV/vis spectrophotometer.

The composition of the resulting SOA extracts was probed using electrospray ionization mass spectrometry (ESI-MS) in negative ion mode. A sample negative ion mode ESI-MS spectrum can be found in the Supporting Information. The observed spectra were complex, with hundreds of peaks packed within the range of the ESI-MS instrument (100−1000 Dalton). Only a very small fraction of peaks could be assigned to the previously identified products of d-limonene ozonolysis.[19,46]

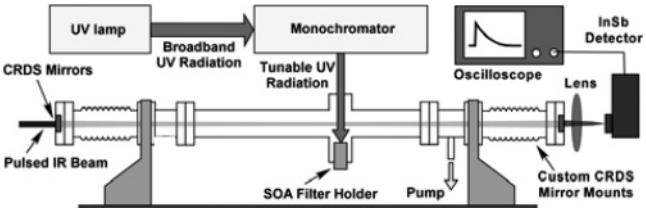

Figure 2. IR−CRDS setup. SOA particles collected on a glass fiber filter are placed in a quartz flow tube and are exposed to tunable UV radiation. Gas-phase products are detected using IR−CRDS along the flow tube axis.

Unassigned peaks occurring at m/z > 200 Dalton are likely to correspond to oligomeric species found in aged SOA particles.[25,26,28,43,47,48] On the whole, the SOA appeared to be more oxidized than that observed in recent chamber studies of limonene ozonolysis,[33,42,44,49] with products corresponding to oxidation of both double bonds in limonene appearing in the mass spectrum. A detailed investigation of the mass spectrum using MS/MS techniques is currently in progress and will be reported elsewhere.

For photolysis experiments, filters with freshly collected particles were placed in a sample holder for analysis using the infrared cavity ring-down spectroscopy (IR−CRDS) system shown in Figure 2. The IR−CRDS system has been described elsewhere,[50,51] but it was modified slightly to accept filters with collected SOA as samples. Briefly, the apparatus consists of a cavity created by two highly reflective mirrors (99.98% at 3.3 μm; suitable for detection of C−H stretching vibrations in organic molecules) spaced by approximately 60 cm. A quartz sample tube (15-mm ID) is located between the mirrors, and the cavity is pumped by an infrared optical parametric oscillator laser. The SOA particles collected on a filter are exposed to UV radiation from a Xenon lamp passed through a 295-nm high-pass filter or, for wavelength-dependent experiments, a monochromator with ∼10 nm resolution. An optoacoustic reference spectrum of HCOOH vapor (1 Torr of HCOOH in 10−100 Torr N_2 buffer) is recorded in parallel with each IR−CRDS spectrum for wavelength calibration purposes.

The system was operated in one of two modes, depending on the goals of the experiment. In the first mode, the particles were exposed to UV light and the IR wavelength was scanned to identify gas-phase reaction products via their unique rovibrational transitions. Alternatively, the IR wavelength was kept constant, and the production of a specific photolysis product, formic acid in these experiments, was measured as a function of UV wavelength to obtain a photodissociation action spectrum. All photolysis experiments were carried out at room temperature (298 K) under slow flow conditions (∼1−5 s cavity flushing time) using ultrahigh purity nitrogen as a bath gas at 7−9 Torr. Before photolysis, the SOA on the filter was allowed to sit in darkness at low pressure for ∼10−15 min. The background signal was very low over this time period, indicating that evaporation of particle components to the gas phase was minimal.

Results

a. UV Absorption Spectra. Figure 3a compares the UV absorption spectrum obtained by wet collection of SOA particles with that of a limonene reference solution. To ensure a meaningful comparison, the limonene mass concentration (110 mg/L) in the reference solution is kept roughly equal to the mass concentration of reacted limonene in the SOA extract. The latter is estimated from the measured particle collection ef-

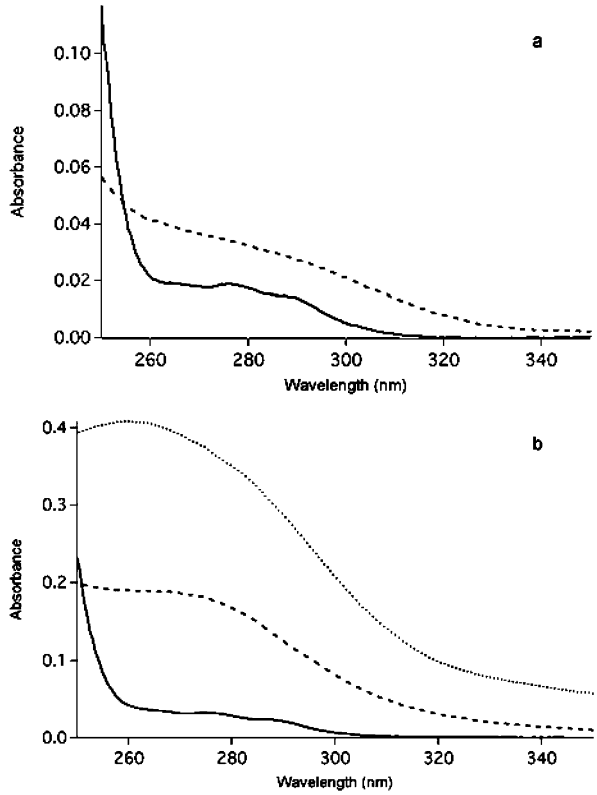

Figure 3. (a) UV/vis spectra of reference limonene solution (solid) and SOA generated from the ozone-initiated oxidation of limonene (dashed), collected by bubbling through dichloromethane. (b) UV/vis spectra of reference limonene solution (solid) and SOA collected on glass fiber filters and ultrasonically extracted into dichloromethane (long dash) and methanol (short dash). The absorbance by limonene is strongly red-shifted by oxidation.

ficiency and from a simplifying assumption that a large mass fraction of oxidized limonene products ends up in the SOA particles. This assumption is reasonable as ozonolysis of limonene at ppm concentrations is expected to produce SOA in fairly high mass yields.[20] Figure 3b similarly compares UV absorption spectra of limonene and of SOA particles collected on filters and ultrasonically extracted with either methanol or dichloromethane.

The absorption spectra of the SOA extracts are characterized by a smooth decrease in the absorption cross section between 250 and 350 nm, and they are clearly different from the spectrum of the parent terpene molecule. The most obvious change is the large red-shift in the SOA spectra, which is observed for SOA extracted with both polar (methanol) and nonpolar (dichloromethane) solvents. The red-shift significantly increases the overlap with the solar spectral radiant flux density, which is dominated by wavelengths in excess of 300 nm in the lower atmosphere.

To assess the impact of RH on the photochemical properties of SOA particles, the UV absorption spectra of SOA prepared at RH <5% and 75% were also compared. These spectra had a similar shape to the ones shown in Figure 3, but the absolute absorbance of the particles prepared at elevated RH was reproducibly larger than for those prepared in dry air. This observation is consistent with the increase in the mass yield of SOA from limonene ozonolysis by a factor of 2−3 at elevated RH (85% vs <2%),[42] which was confirmed by our own measurements. Indeed, the total particle number concentration prepared at elevated RH was on occasions almost an order of magnitude larger than that for dry conditions. The particle size

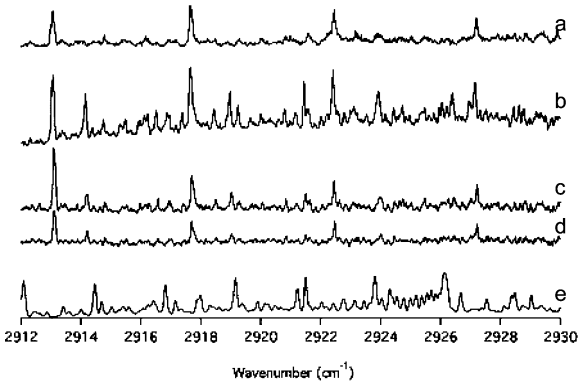

Figure 4. Representative IR−CRDS spectra resulting from the broad photolysis (λ > 295 nm) of limonene SOA particles. (a) Formic acid reference optoacoustic spectrum. (b) Sample spectra taken at $t = 0$ min, (c) 10 min, and (d) 20 min after photolysis. (e) Formaldehyde reference spectrum.

distribution shifted slightly toward smaller particles, with a mean particle diameter of ∼270 nm for 75% RH and ∼320 nm for <5% RH, resulting in the RH-induced enhancement in the total particle mass by a factor of 2−6, in qualitative agreement with data from ref 42.

b. Photodissociation Action Spectra. Limonene SOA collected on glass fiber filters were photolyzed with a broad-band UV source (λ > 295 nm) in the IR−CRDS setup shown in Figure 2. The resulting IR spectra of gas-phase photolysis products (Figure 4) contained characteristic rovibrational lines that could be unambiguously assigned to formic acid and formaldehyde on the basis of an explicit comparison with their reference IR spectra. We explicitly verified that formic acid and formaldehyde emissions were not caused by radiative heating of the sample. Furthermore, there were no formic acid and formaldehyde lines observed from a clean filter, from a clean filter exposed to either ozone or UV radiation, or from unoxidized limonene adsorbed on a filter exposed to UV radiation.

It is likely that larger volatile organic molecules were also emitted by the SOA sample before or during photolysis. However, molecules containing more than 2−3 non-hydrogen atoms are not expected to have rotationally resolved spectra at the 0.1 cm^{-1} resolution of the IR laser. Such molecules contribute to the background absorbance that changes with IR wavelength slowly (typical width of a CH-stretching IR band is 20−30 cm^{-1}) and that is hard to distinguish from instrumental drifts in the cavity ring-down time. The "bump" underlying resolved rotational lines in trace b of Figure 4 may be the result of such unresolved absorption by gas-phase products of SOA photolysis that are larger than formaldehyde and formic acid. Figure 4 shows that the unresolved absorbance is not overwhelmingly large and that it disappears from the IR spectra after 10−20 min of photolysis. We are currently studying the nature of these unidentified photolysis products with mass-spectrometric techniques; results of this study will be reported elsewhere.

Figure 4 reveals that the IR spectrum changed with photolysis time as a result of photobleaching of the SOA sample or secondary photochemical processes occurring on the filter. Under present experimental conditions, the formic acid signal decayed with a time constant of about 30 min. The formaldehyde signal disappeared somewhat faster, suggesting that it came from a different photochemical precursor than formic acid. Secondary photolysis of formaldehyde that was produced by photolysis, but did not immediately desorb from the filter, may also have

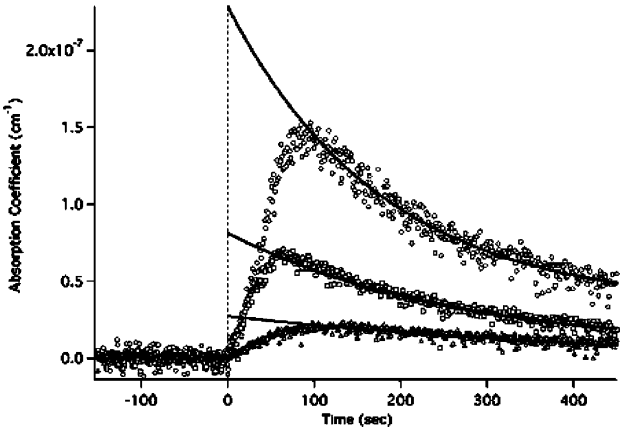

Figure 5. IR−CRDS signals as a function of photolysis time for representative photolysis wavelengths (○ 270 nm; □ 290 nm; △ 310 nm).

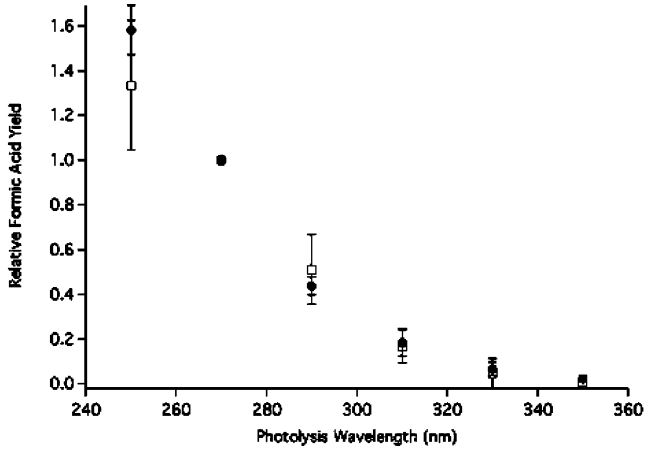

Figure 6. Action spectra of limonene SOA prepared at <5% RH (●) and 75% RH (□). The data were arbitrarily normalized to the formic acid signal observed at 270 nm.

contributed to the more rapid decay of the formaldehyde signal. Secondary photolysis of gas-phase products can be ruled out because of the short CRDS cell flushing time (1−5 s).

Because of photobleaching, the photodissociation action spectrum could not be obtained by simply exposing one and the same SOA sample to different photolysis wavelengths and recording the IR spectrum of the resulting gas-phase products. To circumvent this problem, SOA particles were simultaneously collected from the reaction chamber on six separate filters. Each filter was then placed in the IR−CRDS setup and was exposed to a different photolysis wavelength under otherwise identical conditions. The amount of photolysis products observed at every UV wavelength was normalized to that observed at an arbitrarily selected reference wavelength of 270 nm, allowing for an easy comparison of action spectra obtained under different SOA generation conditions.

The signal measured as a function of the UV irradiation wavelength at a strong formic acid absorption line at ∼2816 cm^{-1} was used as a measure of relative SOA photolysis rates. Figure 5 shows this signal for different photolysis wavelengths as a function of photolysis time. The signal follows a characteristic exponential rise and decay curve. The decay time (5−10 min) can be attributed to the photobleaching of the sample. The rise time (40−50 s) is controlled by a combination of CRDS cell purging (∼2 s) and establishment of equilibrium between gas-phase and wall-adsorbed formic acid.

The decaying portion of the traces shown in Figure 5 was extrapolated to zero time to obtain the wavelength-dependent relative photolysis rate before the SOA sample was significantly affected by photobleaching. Figure 6 shows the resulting relative yields of formic acid during photolysis of limonene SOA as a function of UV photolysis wavelength (i.e., photodissociation action spectrum). All data were normalized to the 270-nm formic acid signal as described above and were further corrected for the intensity of the photolysis light (assuming that the photolysis signal is linear in photolysis power).

The effect of relative humidity on the photodissociation action spectrum was also investigated using limonene SOA. As shown in Figure 6, the shape of the action spectra for limonene-derived SOA prepared in dry air (<5% RH) and at 75% RH is very similar, indicating that humidity has little to no effect on the wavelength dependence of the formic acid yield. The absolute photodissociation yields of formic acid at different humidities could not be straightforwardly compared. UV absorption spectra for SOA prepared in dry air and at elevated relative humidity also had similar shapes but different absolute values.

Discussion

The results of this investigation indicate that solar radiation may play a significant role in the processing of SOA in the atmosphere. Indeed, the absorption spectrum of SOA generated by oxidation of limonene (Figure 3) shows measurable absorbance in the actinic region of the solar spectrum, that is, at wavelengths capable of reaching the lower atmosphere ($\lambda >$ 295 nm). Clearly, the oxidation products that condense to form the SOA particles must contain functional groups capable of absorbing mild UV radiation, a key prerequisite for photochemistry in atmospheric aerosol particles. UV radiation has already been shown to have an effect on the yield of terpene-derived SOA,[31,33,43−45] and this work shows that radiation continues to affect the chemical composition of SOA after particle formation.

The absorption spectrum in Figure 3 can be used to obtain an order of magnitude estimate of the effective absorption cross section of oxidized limonene molecules. For example, dissolved SOA particles absorb roughly as much radiation at 300 nm as an approximately equivalent amount of limonene does at 280 nm. The latter is characterized by an absorption cross section of 3.6×10^{-20} cm^2 $molec^{-1}$ ($\epsilon = 21.6$ L mol^{-1} cm^{-1}, estimated from the reference spectrum shown in Figure 3). Although this is not a huge value, photochemistry in the lower atmosphere is often driven by similarly weak absorptions in the actinic region. For example, the absorption cross section of acetone at 300 nm is 2.77×10^{-20} cm^2 $molec^{-1}$, and this is sufficient to make the lifetime of acetone in the upper troposphere be controlled by photolysis and also to make acetone a significant source of HO_x.[52]

It is instructive to estimate the effective photolysis lifetime for molecules in limonene SOA particles. The photolysis rate constant, $k_p = \int_\lambda \phi(\lambda)\sigma(\lambda)F(\lambda)d\lambda$, can be calculated from the wavelength-dependent quantum yield, $\phi(\lambda)$, absorption cross section, $\sigma(\lambda)$, and solar radiant flux density, $F(\lambda)$, convoluted over the relevant wavelength range. The photolysis lifetime is simply the inverse of the photolysis rate constant. Using the absorption cross sections obtained by scaling the measured relative photodissociation cross sections shown in Figure 6 to the estimated 300-nm value results in a photolysis lifetime of about 4.7×10^5 s, calculated for zero solar zenith angle, "best estimate" surface albedo, and a photolysis quantum yield of unity.[2,53]

Reaction with hydroxyl radical is likely to be the most important competing aging mechanism for organic species

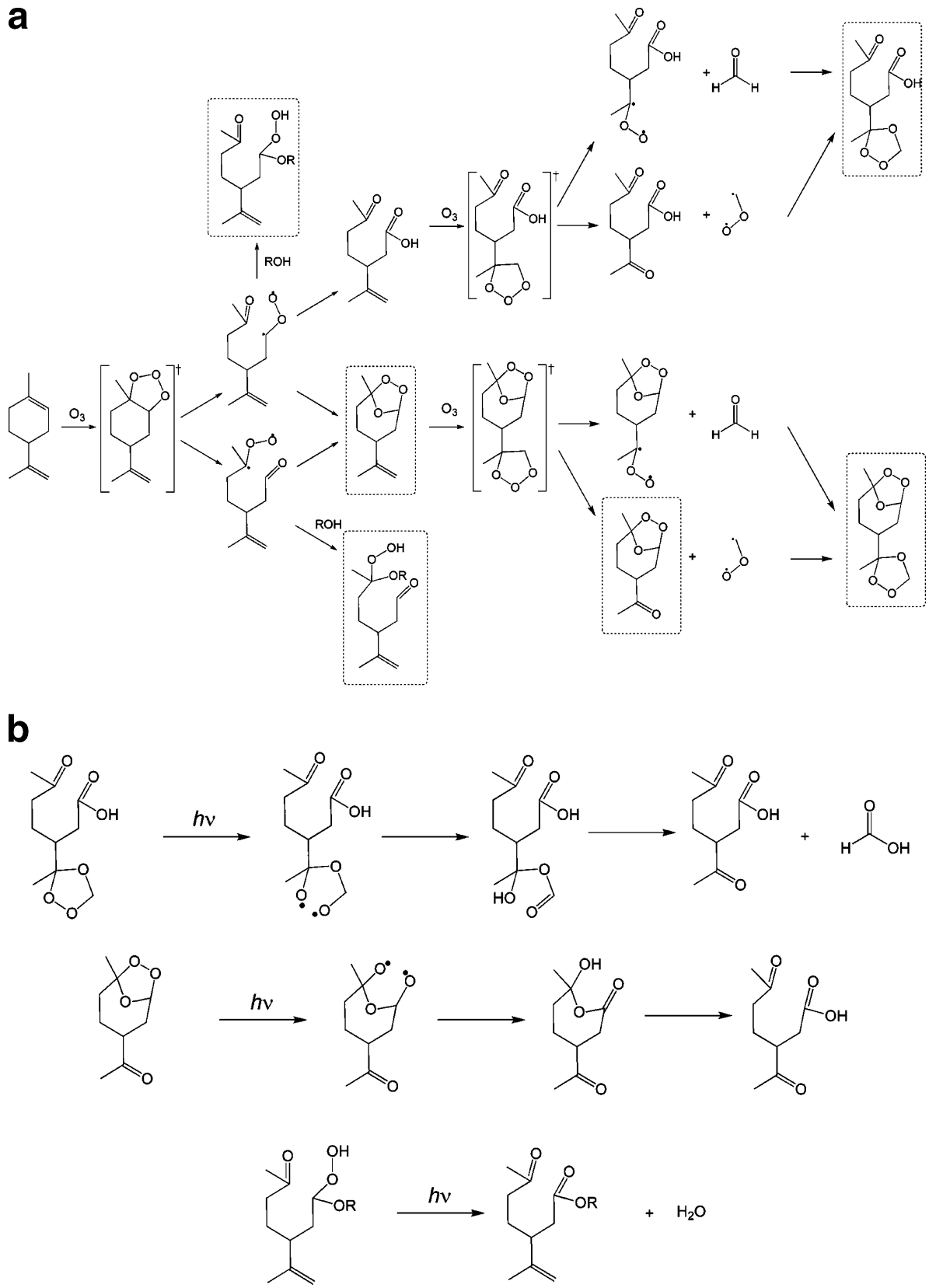

Figure 7. (a) Formation of various peroxides in the ozonolysis of limonene and (b) examples of subsequent photolysis reactions of peroxides, including the formation of formic acid observed using IR−CRDS. Crosses (†) indicate short-lived primary ozonides. Dashed boxes indicate comparatively stable organic peroxides that are susceptible to photolysis in the actinic region.

within the SOA particles. For [OH] = 10^6 molec cm^{-3}, the lifetime of SOA organics with respect to OH attack should be about 10^5 s (assuming a surface reaction probability for OH of 0.1 on solid organic surfaces).[54] However, only the molecules on the surface of the SOA particles should be susceptible to chemical aging, whereas radiation is likely to penetrate deeper and cause photochemical aging throughout the entire particle. Therefore, the rate of photochemical aging of SOA particles in the atmosphere is likely to be comparable to, if not larger than, the rate of chemical aging due to OH attack.

The ozonolysis of monoterpenes has been studied by many research groups, and the reaction mechanism is reasonably well understood.[27,33,40,42,47,55,56] Among the impressively large number of identified products of ozonolysis of monoterpenes, organic peroxides, aldehydes, and ketones are the most likely candidates for the observed weak optical absorption by SOA in the actinic region.

Limonene molecules possess two unsaturated carbon−carbon bonds with different reactivities toward ozonolysis. The rate constant for the reaction of ozone with the endocyclic double bond is estimated to be more than 1 order of magnitude larger than that for the exocyclic (terminal) double bond.[33] However, both bonds can potentially be oxidized under the present conditions of large excess ozone concentration and long reaction time.

Figure 7a shows some of the reactions that can take place during ozonolysis of limonene (this mechanism is by no means complete; it focuses on the formation of organic peroxides). The initial cycloaddition of ozone to the endocyclic double bond results in a highly reactive primary ozonide (POZ) that can rearrange into a secondary ozonide (SOZ) or decompose into a molecule with carboxyl and carbonyl functionalities. These reactions go through a highly reactive intermediate known as a carbonyl oxide, which can either decompose or react with carboxylic acids, alcohols, and water to form organic peroxides. Most of the condensable reaction products are expected to be better absorbers at $\lambda > 295$ nm than limonene itself, in agreement with our observations (Figure 3).

Whereas ozonolysis of the endocyclic double bond in limonene occurs in the gas phase, ozonolysis of the exocyclic double bond is likely to occur after the first generation products condense into initial SOA particles.[33] The primary difference in the reaction mechanism is that POZ splitting now results in two separate molecules rather than one bifunctional molecule. The other significant difference is that thermal decomposition and isomerization of carbonyl oxides are significantly suppressed in the aerosol particle phase, whereas their reactions with the first-generation products are enhanced. Therefore, the yield of exocyclic SOZ and oligomeric peroxides may actually be higher than that derived from the endocyclic double bond.

The most likely ozonolysis product that can produce formic acid upon photolysis is the secondary ozonide (1,3,4-trioxalone) formed from the ozonolysis of the exocyclic double bond. The photolysis mechanism (Figure 7b) is similar to that of the secondary ozonides of undecylenic acid[50] and other olefins.[51,57,58] It involves breaking the weakest O−O bond in the ozonide, followed by a H-atom transfer and subsequent decomposition. It is not clear what functional group serves as a precursor to formaldehyde, which is also observed by the CRDS setup. It is possible that it results from secondary reactions of OH produced by photolysis of hydroxyhydroperoxides.

A qualitative comparison of the absorption spectrum shown in Figure 3 and the photodissociation action spectrum shown in Figure 6 provides additional insights into the reaction mechanism. If the absorption and action spectra had more similar shapes, this would indicate that production of formic acid results from the photolysis of the primary absorber within the particles. However, if a fit of the action spectrum is appropriately scaled and subtracted from the absorption spectrum, there is remaining signal in the 300-nm region. This confirms the presence of aldehyde and ketone functionalities, both of which absorb UV radiation between about 260 and 310 nm, but do not produce formic acid as a photolysis product.

Conclusion

SOA particles formed from the ozone-initiated oxidation of limonene have been found to absorb radiation in the actinic region of the solar spectrum ($\lambda > 295$ nm). The ozonolysis of limonene's two double bonds produces a variety of functional groups, including carbonyls and peroxides, which are responsible for the increased absorption of UV radiation. Furthermore, the resulting SOA particles are photochemically active in that they emit small volatile molecules upon absorption of actinic radiation. While further work is needed to completely quantify this effect, it is quite probable that such photochemical processes can efficiently compete with other organic aerosol particle aging processes in the atmosphere.

Acknowledgment. The authors wish to thank Dr. John Greaves for his assistance with ESI-MS. This study was supported by the National Science Foundation through the Environmental Molecular Science Institute program, grant CHE-0431312 (formerly CHE-0209719), and the Atmospheric Chemistry Program, grant ATM-0509248. M. L. W. was supported by a National Science Foundation Graduate Research Fellowship and J. P. was supported by a Camille and Henry Dreyfus Fellowship in Environmental Chemistry.

Supporting Information Available: A sample ESI-MS spectrum of the SOA components, a table of masses, and structures of possible products. This material is available free of charge via the Internet at http://pubs.acs.org.

References and Notes

(1) Kanakidou, M.; Seinfeld, J. H.; Pandis, S. N.; Barnes, I.; Dentener, F. J.; Facchini, M. C.; Van Dingenen, R.; Ervens, B.; Nenes, A.; Nielsen, C. J.; Swietlicki, E.; Putaud, J. P.; Balkanski, Y.; Fuzzi, S.; Horth, J.; Moortgat, G. K.; Winterhalter, R.; Myhre, C. E. L.; Tsigaridis, K.; Vignati, E.; Stephanou, E. G.; Wilson, J. *Atmos. Chem. Phys.* **2005**, *5*, 1053.

(2) Finlayson-Pitts, B. J.; Pitts, J. N. *Chemistry of the Upper and Lower Atmosphere: Theory, Experiments, and Applications*; Academic Press: San Diego, CA, 2000.

(3) Pope, C. A., III; Burnett, R. T.; Thun, M. J.; Calle, E. E.; Krewski, D.; Ito, K.; Thurston, G. D. *J. Am. Med. Assoc.* **2002**, *287*, 1132.

(4) Dockery, D. W.; Pope, C. A., III; Xu, X.; Spengler, J. D.; Ware, J. H.; Fay, M. E.; Ferris, B. G., Jr.; Speizer, F. E. *N. Engl. J. Med.* **1993**, *329*, 1753.

(5) Gauderman, W. J.; Gilliland, G. F.; Vora, H.; Avol, E.; Stram, D.; McConnell, R.; Thomas, D.; Lurmann, F.; Margolis, Helene, G.; Rappaport, E. B.; Berhane, K.; Peters John, M. *Am. J. Respir. Crit. Care Med.* **2000**, *166*, 76.

(6) Seinfeld, J. H.; Pandis, S. N. *Atmospheric Chemistry and Physics*: *From Air Pollution to Climate Change*; Wiley: New York, 1998.

(7) Lim, H.-J.; Turpin, B. J. *Environ. Sci. Technol.* **2002**, *36*, 4489.

(8) Alves, C.; Carvalho, A.; Pio, C. *J. Geophys. Res.* **2002**, *107*, ICC7/1.

(9) Duce, R. A.; Mohnen, V. A.; Zimmerman, P. R.; Grosjean, D.; Cautreels, W.; Chatfield, R.; Jaenicke, R.; Ogren, J. A.; Pellizzari, E. D.; Wallace, G. T. *Rev. Geophys. Space Phys.* **1983**, *21*, 921.

(10) Jacobson, M. C.; Hansson, H. C.; Noone, K. J.; Charlson, R. J. *Rev. Geophys.* **2000**, *38*, 267.

(11) Hildemann, L. M.; Markowski, G. R.; Cass, G. R. *Environ. Sci. Technol.* **1991**, *25*, 744.

(12) Liu, D. Y.; Wenzel, R. J.; Prather, K. A. *J. Geophys. Res.* **2003**, *108*, SOS 14/1.

(13) Middlebrook, A. M.; Murphy, D. M.; Thomson, D. S. *J. Geophys. Res.* **1998**, *103*, 16475.

(14) Mochida, M.; Kitamori, Y.; Kawamura, K.; Nojiri, Y.; Suzuki, K. *J. Geophys. Res.* **2002**, *107*, AAC1/1.

(15) Murphy, D. M.; Thomson, D. S.; Mahoney, M. J. *Science* **1998**, *282*, 1664.

(16) Raes, F.; Bates, T.; McGovern, F.; Van, Liedekerke, M. *Tellus B: Chem. Phys. Meteorol.* **2000**, *52B*, 111.

(17) Guenther, A.; Hewitt, C. N.; Erickson, D.; Fall, R.; Geron, C.; Graedel, T.; Harley, P.; Klinger, L.; Lerdau, M.; et al. *J. Geophys. Res.* **1995**, *100*, 8873.

(18) Went, F. W. *Nature* **1960**, *187*, 641.

(19) Leungsakul, S.; Jaoui, M.; Kamens, R. M. *Environ. Sci. Technol.* **2005**, *39*, 9583.
(20) Hoffmann, T.; Odum, J. R.; Bowman, F.; Collins, D.; Klockow, D.; Flagan, R. C.; Seinfeld, J. H. *J. Atmos. Chem.* **1997**, *26*, 189.
(21) Sax, M.; Zenobi, R.; Baltensperger, U.; Kalberer, M. *Aerosol Sci. Technol.* **2005**, *39*, 822.
(22) Koch, S.; Winterhalter, R.; Uherek, E.; Kolloff, A.; Neeb, P.; Moortgat, G. K. *Atmos. Environ.* **2000**, *34*, 4031.
(23) Bonn, B.; Schuster, G.; Moortgat, G. K. *J. Phys. Chem. A* **2002**, *106*, 2869.
(24) Czoschke, N. M.; Jang, M.; Kamens, R. M. *Atmos. Environ.* **2003**, *37*, 4287.
(25) Gao, S.; Ng, N. L.; Keywood, M.; Varutbangkul, V.; Bahreini, R.; Nenes, A.; He, J.; Yoo, K. Y.; Beauchamp, J. L.; Hodyss, R. P.; Flagan, R. C.; Seinfeld, J. H. *Environ. Sci. Technol.* **2004**, *38*, 6582.
(26) Gao, S.; Keywood, M.; Ng, N. L.; Surratt, J.; Varutbangkul, V.; Bahreini, R.; Flagan, R. C.; Seinfeld, J. H. *J. Phys. Chem. A* **2004**, *108*, 10147.
(27) Iinuma, Y.; Boge, O.; Gnauk, T.; Herrmann, H. *Atmos. Environ.* **2004**, *38*, 761.
(28) Baltensperger, U.; Kalberer, M.; Dommen, J.; Paulsen, D.; Alfarra, M. R.; Coe, H.; Fisseha, R.; Gascho, A.; Gysel, M.; Nyeki, S.; Sax, M.; Steinbacher, M.; Prevot, A. S. H.; Sjogren, S.; Weingartner, E.; Zenobi, R. *Faraday Discuss.* **2005**, *130*, 265.
(29) Bahreini, R.; Keywood, M. D.; Ng, N. L.; Varutbangkul, V.; Gao, S.; Flagan, R. C.; Seinfeld, J. H.; Worsnop, D. R.; Jimenez, J. L. *Environ. Sci. Technol.* **2005**, *39*, 5674.
(30) Tolocka, M. P.; Jang, M.; Ginter, J. M.; Cox, F. J.; Kamens, R. M.; Johnston, M. V. *Environ. Sci. Technol.* **2004**, *38*, 1428.
(31) Presto, A. A.; Huff, Hartz, K. E.; Donahue, N. M. *Environ. Sci. Technol.* **2005**, *39*, 7036.
(32) Presto, A. A.; Huff, Hartz, K. E.; Donahue, N. M. *Environ. Sci. Technol.* **2005**, *39*, 7046.
(33) Zhang, J.; Huff Hartz, K. E.; Pandis, S. N.; Donahue, N. M. *J. Phys. Chem. A* **2006**, *110*, 11053−11063.
(34) Fan, Z.; Lioy, P.; Weschler, C.; Fiedler, N.; Kipen, H.; Zhang, J. *Environ. Sci. Technol.* **2003**, *37*, 1811.
(35) Rohr, A. C.; Weschler, C. J.; Koutrakis, P.; Spengler, J. D. *Aerosol Sci. Technol.* **2003**, *37*, 65.
(36) Weschler, C. J.; Shields, H. C. *Atmos. Environ.* **1999**, *33*, 2301.
(37) Liu, X.; Mason, M.; Krebs, K.; Sparks, L. *Environ. Sci. Technol.* **2004**, *38*, 2802.
(38) Wainman, T.; Zhang, J.; Weschler, C. J.; Lioy, P. J. *Environ. Health Perspect.* **2000**, *108*, 1139.
(39) Sarwar, G.; Olson, D. A.; Corsi, R. L.; Weschler, C. J. *JAWMA* **2004**, *54*, 367.
(40) Grosjean, D.; Williams, E. L., II; Grosjean, E.; Andino, J. M.; Seinfeld, J. H. *Environ. Sci. Technol.* **1993**, *27*, 2754.
(41) Dalton, C. N.; Jaoui, M.; Kamens, R. M.; Glish, G. L. *Anal. Chem.* **2005**, *77*, 3156.
(42) Jonsson, S. M.; Hallquist, M.; Ljungstroem, E. *Environ. Sci. Technol.* **2006**, *40*, 188.
(43) Surratt, J. D.; Murphy, S. M.; Kroll, J. H.; Ng, N. L.; Hildebrandt, L.; Sorooshian, A.; Szmigielski, R.; Vermeylen, R.; Maenhaut, W.; Claeys, M.; Flagan, R. C.; Seinfeld, J. H. *J. Phys. Chem. A* **2006**, *110*, 9665.
(44) Ng, N. L.; Kroll, J. H.; Keywood, M. D.; Bahreini, R.; Varutbangkul, V.; Flagan, R. C.; Seinfeld, J. H.; Lee, A.; Goldstein, A. H. *Environ. Sci. Technol.* **2006**, *40*, 2283.
(45) Kroll, J. H.; Ng, N. L.; Murphy, S. M.; Flagan, R. C.; Seinfeld, J. H. *Environ. Sci. Technol.* **2006**, *40*, 1869.
(46) Warscheid, B.; Hoffmann, T. *Rapid Commun. Mass Spectrom.* **2001**, *15*, 2259.
(47) Docherty, K. S.; Wu, W.; Lim, Y. B.; Ziemann, P. J. *Environ. Sci. Technol.* **2005**, *39*, 4049.
(48) Iinuma, Y.; Boege, O.; Miao, Y.; Sierau, B.; Gnauk, T.; Herrmann, H. *Faraday Discuss.* **2005**, *130*, 279.
(49) Leungsakul, S.; Jeffries, H. E.; Kamens, R. M. *Atmos. Environ.* **2005**, *39*, 7063.
(50) Gomez, A.; Park, J.; Walser, M.; Lin, A.; Nizkorodov, S. A. *J. Phys. Chem. A* **2006**, *110*, 3584.
(51) Park, J.; Gomez, A. L.; Walser, M. L.; Lin, A.; Nizkorodov, S. A. *Phys. Chem. Chem. Phys.* **2006**, *8*, 2506.
(52) Wennberg, P. O.; Hanisco, T. F.; Jaegle, L.; Jacob, D. J.; Hintsa, E. J.; Lanzendorf, E. J.; Anderson, J. G.; Gao, R. S.; Keim, E. R.; Donnelly, S. G.; Del, Negro, L. A.; Fahey, D. W.; McKeen, S. A.; Salawitch, R. J.; Webster, C. R.; May, R. D.; Herman, R. L.; Proffitt, M. H.; Margitan, J. J.; Atlas, E. L.; Schauffler, S. M.; Flocke, F.; McElroy, C. T.; Bui, T. P. *Science* **1998**, *279*, 49.
(53) Sander, S. P.; Friedl, R. R.; Golden, D. M.; Kurylo, M. J.; Huie, R. E.; L., O. V.; Moortgat, G. K.; Ravishankara, A. R.; Kolb, C. E.; Molina, M. J.; Finlayson-Pitts, B. J. *Chemical Kinetics and Photochemical Data for Use in Stratospheric Modeling: Evaluation Number 14*; Jet Propulsion Laboratory: Pasadena, CA, 2003.
(54) Bertram, A. K.; Ivanov, A. V.; Hunter, M.; Molina, L. T.; Molina, M. J. *J. Phys. Chem. A* **2001**, *105*, 9415.
(55) Dekermenjian, M.; Allen, D. T.; Atkinson, R.; Arey, J. *Aerosol Sci. Technol.* **1999**, *30*, 349.
(56) Griesbaum, K.; Hilss, M.; Bosch, J. *Tetrahedron* **1996**, *52*, 14813.
(57) Hawkins, M.; Kohlmiller, C. K.; Andrews, L. *J. Phys. Chem.* **1982**, *86*, 3154.
(58) Andrews, L.; Kohlmiller, C. K. *J. Phys. Chem.* **1982**, *86*, 4548.